JTTEE5 15:796-801
DOI: 10.1361/105996306X1468794
1059-9630/$19.00 © ASM International

Peer Reviewed

Scientific, Technological, and Economic Aspects of Rapid Tooling by Electric Arc Spray Forming

P.S. Grant, S.R. Duncan, A. Roche, and C.F. Johnson

(Submitted March 7, 2006; in revised form June 23, 2006)

For the last seven years, Oxford University and Ford Motor Company personnel have been researching jointly the development of the large-scale spray forming of steel tooling capable for use in mass production, particularly for the pressing of sheet metal in automotive applications. These investigations have involved: the comprehensive microstructure and property studies, modeling of shape evolution and heat flow, real-time feedback control of tool temperature to eliminate tool distortion, high-speed imaging and particle image velocimetry of droplet deposition on three-dimensional (3D) shapes, testing of full-scale tools for different applications in the production environment, and detailed studies of the cost and time savings realized for different tooling applications. This paper provides an overview of the scientific and technical progress to date, presents the latest results, and describes the current state-of-the-art. Many of the insights described have relevance and applicability across the family of thermal spray processes and applications.

Keywords diagnostics and control, substrate temperature during thermal spray process, thermal and phase coatings

1. Introduction

In the development of a new mass-produced automotive vehicle, the provision of the tooling is frequently the longest lead-time item. The large press tooling sets that press steel or aluminum (Al) sheets to form large body panels can take six to nine months to manufacture. These production tooling sets then can produce up to 1 million components. Large tool sets also represent a significant fraction of the overall investment required to introduce a new vehicle model. Most volume-capable tooling is manufactured by the computer numeric controlled (CNC) machining of either gray iron/Al castings or billet material. Computer numeric controlled practices and technology are well established and are optimized to produce robust tools of high tolerances, but with the previously mentioned prolonged lead times. A radical alternative to CNC machining for the manufacture of tooling is based on the selective addition of steel onto a sacrificial pattern using electric arc spray forming. While spray forming is established for soft zinc-base prototyping tools (Ref 1), the spray forming of steel offers the potential to manufacture tools of sufficient quality and robustness for production applications at reduced time and cost.

The spray forming of tooling involves the deposition of molten steel droplets onto a freeze-cast alumina substrate (Ref 2) or other robust substrate (Ref 3). The freeze-cast substrate is sprayed using four electric arc spray guns mounted on a six-axis programmable robot, as shown in Fig. 1. A robot moves the guns and their metal sprays in a controlled way termed the "path plan" over the surface of the freeze-cast substrate. Figure 2 shows the spray forming process during the manufacture of a 10 mm thick, 300 by 300 mm steel shell. After spraying, the sprayed shell undergoes trimming, backing, and bolstering before entering production service. This paper gives an overview of some of the key findings from investigations of the spray forming process for tooling applications involving the Departments of Materials and Engineering Science at Oxford University, U.K., and the Ford Motor Company, Dearborn, MI.

2. Dimensional Accuracy

The manufacture of steel tooling by spray forming is usually frustrated by the excessive warping and distortion of the steel shells during manufacture and during cooling to room temperature. To understand this behavior better, experiments were performed in which the average surface temperature of 300 by 300 by up to 10 mm Fe-0.8wt.%C steel shells was controlled carefully throughout spraying, and any deflection or distortion of the shell was monitored using a linear displacement sensor on the substrate back face. For each temperature investigated, the freeze-cast ceramic substrates were preheated to the control temperature using an array of infrared (IR) heaters to eliminate thermal transients at the beginning of spraying. Figure 3 shows the resulting variation in deflection of the shell as a function of the

This article was originally published in *Building on 100 Years of Success, Proceedings of the 2006 International Thermal Spray Conference* (Seattle, WA), May 15-18, 2006, B.R. Marple, M.M. Hyland, Y.-Ch. Lau, R.S. Lima, and J. Voyer, Ed., ASM International, Materials Park, OH, 2006.

P.S. Grant, Department of Materials, Oxford University, Parks Rd, Oxford OX1 3PH, U.K.; **S.R. Duncan,** Department of Engineering Science, Oxford University, Parks Rd, Oxford OX1 3PJ, U.K.; and **A. Roche** and **C.F. Johnson,** Scientific Research Laboratory, Ford Motor Co., Dearborn, MI 48124. Contact e-mail: Patrick.grant@materials.ox.ac.uk.

Fig. 1 Spray cell at Oxford University featuring four electric arc spray guns and a six-axis robot

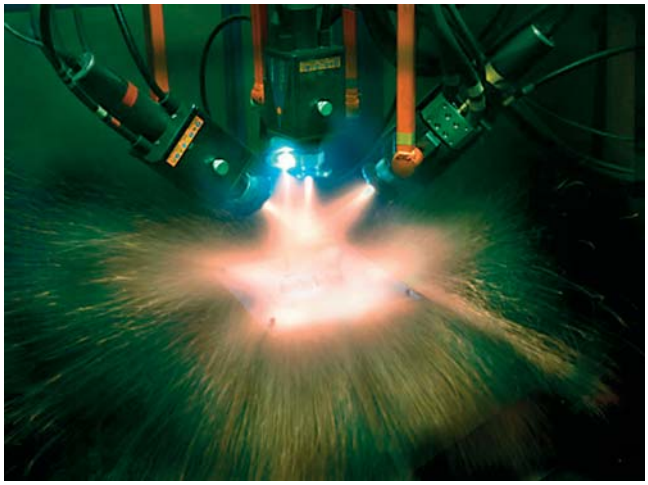

Fig. 2 Spray forming process in operation

steady-state top surface temperature measured by thermal imaging. Two temperatures of approximately 215 and 365 °C were identified where there was little or no deflection of the shell. As described in more detail elsewhere (Ref 4), at 365 °C, the rate of evolution of bainite in the steel microstructure and the associated volume changes and transformation strains approximately balanced the rate of thermal contraction of the shell due to cooling from the spray temperature. At 215 °C, the shell initially deflected due to the evolution of tensile stresses in the shell; however, eventually the bainite began to form from the metastable austenite, and the tensile stresses were relieved progressively (Ref 4). Compared with the 365 °C temperature, bainite formation at 215 °C was much more sluggish. At 365 °C, the achievable thickness of the shell is more or less unlimited because the rate of bainite formation balances the rate of thermal contraction throughout. At 215 °C, zero net distortion occurs from the balancing of the initial tensile contraction of the shell and the subsequent compressive transformation stresses, and so depends on the final shell thickness. In other words, the shell initially distorts in a tensile manner, but once bainite starts to form after an incubation period, the shell distortion reverses progressively as more bainite is formed. Provided the spraying stops at the moment when the overall shell distortion is instantaneously zero, shells with no distortion can be obtained.

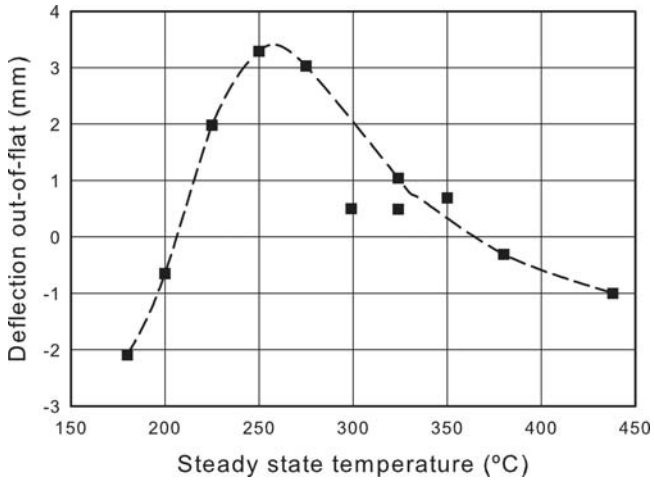

Fig. 3 Net 300 by 300 by ~10 mm Fe-0.8wt.%C shell distortion at room temperature as a function of the controlled average steady-state temperature measured during manufacture by thermal imaging

3. Temperature Distribution

Having determined experimentally the shell average temperature that provides the key stress relieving transformations in the steel microstructure, it was then necessary to impose that "control" temperature at all points of the shell as it forms. If significant lateral temperature gradients were to develop, then the rate of thermal contraction/expansion will vary from place to place and will provide a driving force for distortion. Since the multiple sprays impacting on the surface were themselves the primary source not only of mass and heat, but also of cooling due to the high-pressure N_2 gas streams used for atomization, it was evident that the robot motion that moved the spray guns, termed the "path plan," would have a major role in determining the lateral distribution of temperature. For instance, it was obvious that the faster the robot can move across the surface, the lower will then be the lateral temperature gradients. However, the effect of other path plan parameters on thermal distributions was harder to anticipate.

The surface thermal variations induced by simple two-dimensional (2D) path plans can be analyzed mathematically. For example, Fig. 4 shows a typical "raster" (Fig. 4a) and a "mirror-box" (so termed because the path is reflected at box edges) (Fig. 4b) path plan. Raster patterns are used widely in the thermal spray community to produce coatings of constant thickness. During the execution of the path plan, the arc spray gun cluster moved sequentially from point to point, before returning to the start point and repeating the pattern many times. Robot velocities over the surface were typically 50 to 400 mm/s and spray

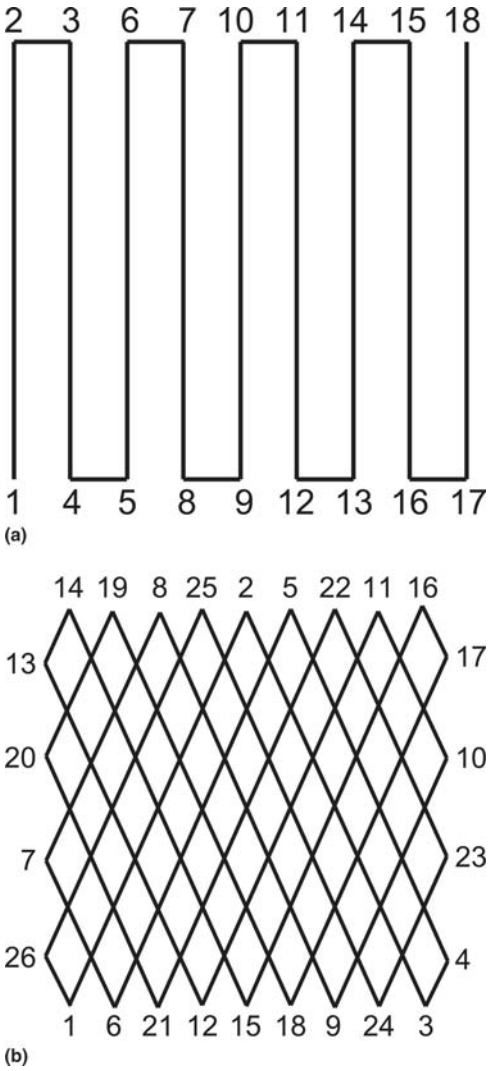

Fig. 4 Schematic representation of (a) raster and (b) "mirror-box" path plans

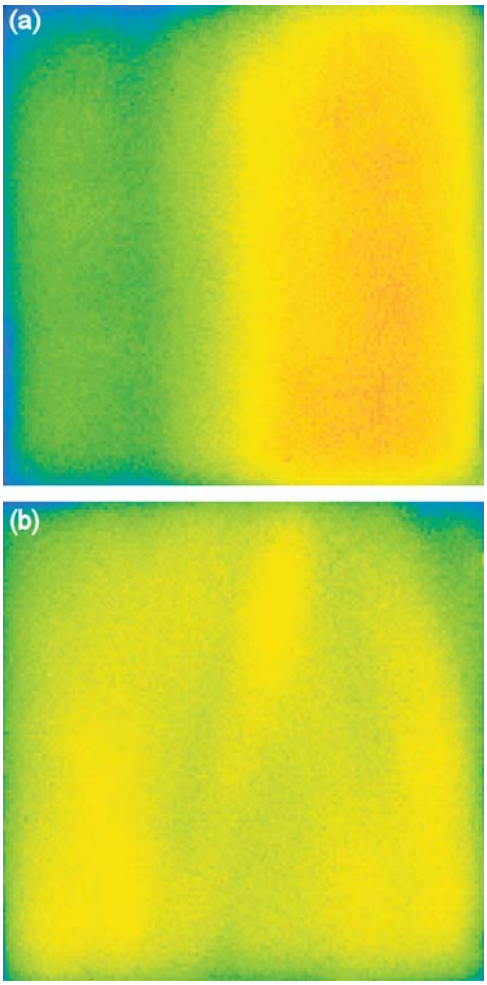

Fig. 5 Temperature distribution over a 300 by 300 mm Fe-0.8wt.%C shell measured by thermal imaging for the path plans in (a) Fig. 4(a) and (b) Fig. 4(b). The average temperature is 365 °C in both cases.

distances were 100 to 200 mm. Although the raster pattern in Fig. 4(a) will produce shells of acceptable uniform thickness at the end of spraying, it will induce relatively strong left-to-right thermal gradients at the midpoint of the path plan. The induction of lateral temperature gradients can be considered as the excitation of periodic thermal variations with respect to distance, in this case with a wavelength similar in length to the shell width. According to analysis (Ref 5), the mirror-box path plan in Fig. 4(b) shows more isotropic thermal variations of shorter wavelength, provided the position and the angle from which the path is "launched" are carefully selected.

Figure 5 shows experimental thermal images taken at the same instant midway through a raster (Fig. 5a) and mirror-box (Fig. 5b) path plan, during the spraying of Fe-0.8wt.%C 300 by 300 mm steel shells under otherwise constant process parameters. The thermal imaging camera viewed the shell top surface from above in real time, and to obtain these images the robot was moved out of the field of view for 1 s so that an unobscured frame of the shell surface could be recorded. In each case, the color relates to the instantaneous surface temperature of the sprayed shell, and the average surface temperature was the same in both cases at 365 °C. Comparison of Fig. 5(a) and (b) shows that, as predicted, the mirror-box path plan produced a substantially more homogeneous thermal distribution.

4. Online Thermal Control

Even when optimized robot path plans are selected and programmed at the beginning of the spray forming process, some real-time monitoring and regulation of the spray process is needed once spraying begins. In this case, the average surface temperature is the process characteristic requiring control since Fig. 3 showed that surface temperature was a suitable proxy for tool deflection and distortion. A flexible, robust system for the direct real-time measurement of distortion was considered to be unavailable, whereas the surface temperature of the sprayed shell has been shown to be relatively easy to measure by thermal imaging (Fig. 5a and b) (Ref 6). A series of studies were then undertaken to identify those electric arc spray parameters that:

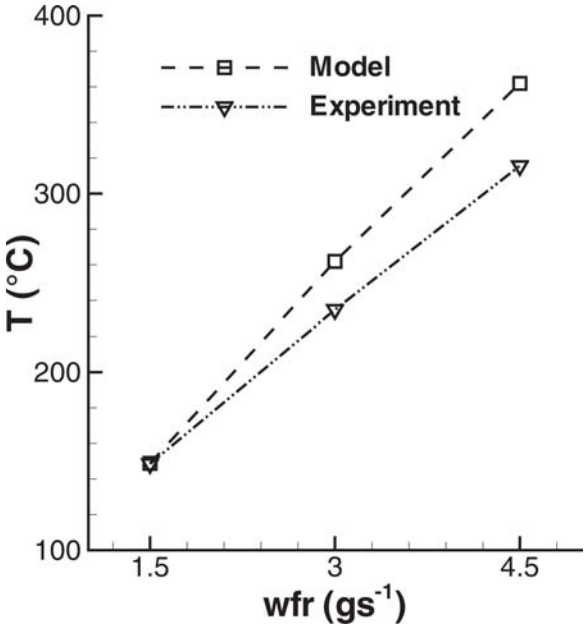

Fig. 6 Average shell top surface temperature as a function of the wire feed rate (wfr) to each of the four electric arc spray guns under otherwise identical conditions

(a) could provide a predictable and useful change in average shell surface temperature and (b) could be actuated with a frequency and sensitivity appropriate for the dynamics of the process (Ref 7). Figure 6 shows the variation in average shell top surface temperature for a 300 by 300 mm Fe-0.8wt.%C shell as a function of the wire feed rate (wfr, g/s) to each of the four spray guns, under otherwise constant spray conditions.

As the wire feed rate changed from 1.5 to 4.5 g/s, the average surface temperature increased from ~145 to ~310 °C in an approximately linear fashion. Figure 6 also shows the results of numerical simulations of the average surface temperature, utilizing measurements of the spray arrival temperature (Ref 8), surface heat transfer coefficient distribution, and other boundary conditions (Ref 9), showing good agreement with the experimental data over the range. Because spray formed tooling shells are generally relatively wide but thin (at least 300 by 300 mm with a maximum thickness of 15 mm), and because the relatively high thermal conductivity steel shell is formed on an insulating ceramic substrate, through-thickness temperature gradients could safely be assumed to be negligible in shell heat flow simulations.

A control system based on thermal imaging measurements of the average shell surface temperature and its regulation by manipulation of the wire feed rate to each of the four guns in real time was implemented (Ref 7). Figure 7 shows a typical response of the sprayed shell average surface temperature as a function of time, while under closed-loop control for the temperature. After an initial thermal transient in the first 100 s where there was some thermal equilibration between the initial layers of sprayed steel and the freeze-cast substrate, the closed-loop feedback control system maintained the average shell top surface temperature to within ±3 °C of the target temperature, by automatic corrections in the wire feed rate.

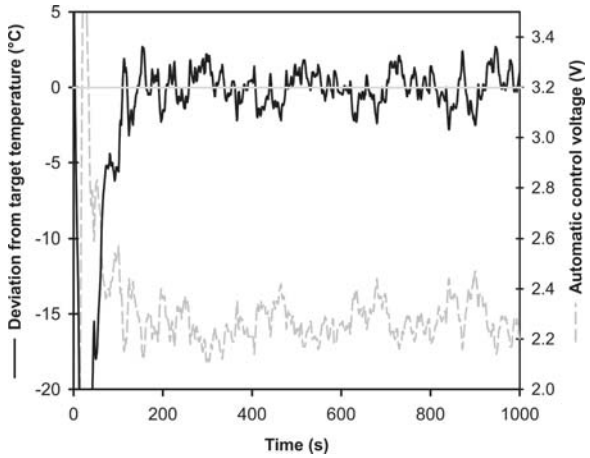

Fig. 7 Average shell surface temperature deviation from target during the manufacture of a Fe-0.8wt.%C 300 by 300 by 10 mm shell and associated automatic changes in control voltage that was directly proportional to the wire feed rate

5. Deposit Structure

The microstructure of as-sprayed steel shells produced by electric arc spraying comprised distinct steel splats, delineated by oxide and porosity. Although the N_2 gas that atomized and projected the liquid steel droplets provided some "shrouding" from the oxygen that was always present in the high flow rate of the cross-flow air to remove fines and fume, this could not prevent some oxidation of the droplets. Low fractions of porosity (<5%) were generally of little consequence to tool performance, but when porosity fractions rose around certain topographic features, the mechanical and thermal performance of the tool could be compromised. The mechanism by which macroporosity developed in these regions was shown by high-speed, high-magnification imaging to be a complex process, involving splashing of the sprayed steel droplets as they impacted the surface and the redeposition of the smaller splash droplets (Ref 10). For example, Fig. 8 shows the formation of a bridge in the vicinity of a relatively narrow substrate feature; whereas on other regions of the same substrate, the sprayed steel has penetrated and replicated fully all the geometric features.

To understand splashing, redeposition, and bridging, particle image velocimetry (PIV) was used. In PIV, a frozen image of the spray droplets within a well-defined 2D plane through the spray is captured on a digital camera by the use of an external short pulse of high-intensity laser light (Ref 11). The laser light is manipulated by an optical arm and lenses to produce a focused plane of light of ~1 mm in thickness. A second image is taken similarly a few milliseconds later, and software identifies droplet image pairs in the two frames so that a vector map of particle velocity in the plane is readily obtained. Figure 9 shows a PIV droplet velocity map in the vicinity of a simple step feature during the electric arc spraying and deposition of Fe-0.8wt.%C droplets. The expected predominantly downward, high-velocity (~70 m/s) flow of primary droplets in regions away from the substrate surface was replaced by velocity vectors indicating the slower, upward, and sideways flow of droplets in the near-substrate region. This upward flow arose because the PIV measurement of the local velocity was derived from the mode of the

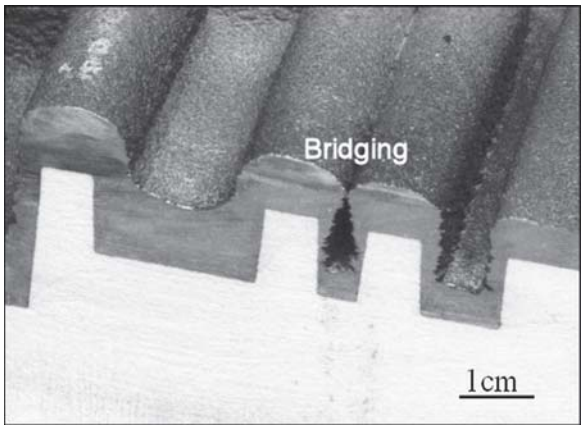

Fig. 8 Freeze-cast substrate and sprayed steel shell showing the effect of narrow features on bridging

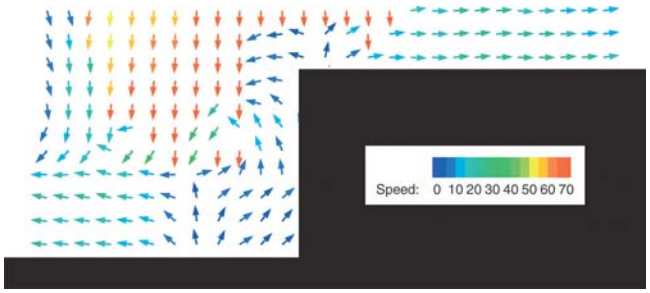

Fig. 9 PIV measurements of arc sprayed Fe-0.8wt.%C droplet velocities (m/s) at a simple 20 mm vertical step geometric feature, indicating the prevalence of droplet splashing during the deposition and the redeposition

local velocity distribution, and since one incoming primary droplet of velocity ~70 m/s and temperature ~2200 °C (Ref 8) generated typically 15 to 20 secondary splash droplets, it was the splash droplets that dominated PIV measurements in the near-surface region. At the left and right extremes of the step geometry, the smaller splash droplets were removed as overspray, seeded in the N_2 flow around the substrate. However, close to the step, some upward and sideways splash droplet trajectories intersected the vertical step wall and redeposition occurred. Because these droplets are relatively small and slow moving, they increased oxide and porosity fractions at the vertical walls. Redeposited droplets in this region also then "shadow" regions of the wall lower down from direct deposition of primary droplets, leading eventually to the formation of macropores and, in extreme cases, the bridging behavior previously shown in Fig. 8.

Simulations were also performed (Ref 12) to identify the minimum feature size that can be replicated, as a function of any particular gun cluster arrangement and robot path plan. Figure 10 shows a simulation of the evolution of the shape and internal porosity in a sprayed steel shell in the case of a simple notch. The simulation included the effects of splashing, redeposition, and shadowing, and captured correctly the development of particular lines of increased porosity radiating from the notch upper corners that were a feature of spray formed microstructures around geometric features under some conditions.

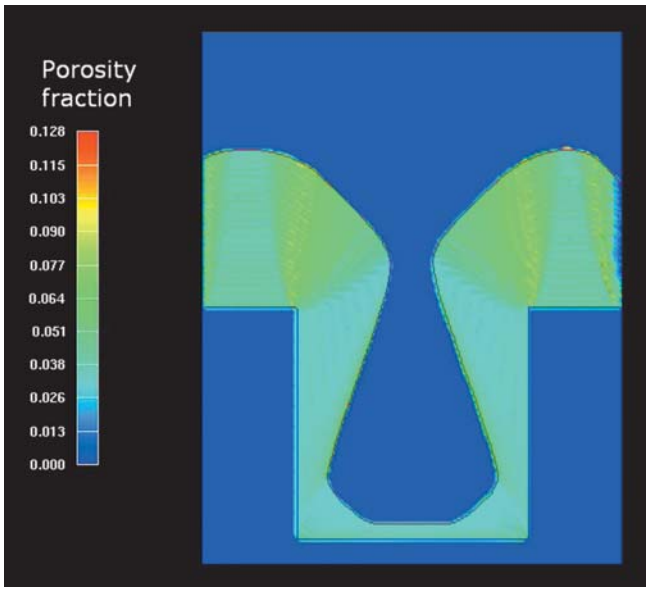

Fig. 10 Simulation of the spray steel shell shape and the porosity fraction evolution in a notch substrate feature

6. Industrial Application

Spray forming of tools is not a general-purpose toolmaking process, but may achieve penetration in markets where the time and cost savings afforded by spray forming are most compelling. The potential market sectors for spray formed tools are shown schematically in Fig. 11 in terms of the technical requirement (dimensional accuracy, sliders, pins, robustness, etc.) and the final proportion of the finished tool cost that is contributed by spray forming (the spray formed content).

In the case of relatively simple rotational molding tools, Fig. 11 shows that a tool made by spray forming contains a relatively high final spray formed content. In the most dimensionally accurate and complex tools for polymer injection molding, the spray formed content is a relatively small fraction of the overall tool cost because more manufacturing steps are required, such as postspray machining, the use of inserts, and so forth. For press tools that are the focus of the current work, overall tool value increases, the spray formed shell content is reduced, but time savings become more compelling, especially for press tools with *x-y* dimensions larger than 400 by 400 mm.

Figure 12 shows a 800 by 600 mm spray formed steel shell with severe, up to 100 mm, changes in height and vertical walls that was subsequently trimmed, backed, and put into service in a commercial sheet steel pressing operation, producing more than 100,000 successful pressings. The shell thickness was typically 15 mm, and this tool represents the largest single-piece steel tool manufactured by spray forming. A further relatively unexplored capability of spray forming is to take a tool used to make prototype parts, but one that is insufficiently robust for volume manufacture, and to use it as a master or pattern for the spray form tool process. Providing dimensional tolerances can be maintained, this may offer a particular economic attraction since most of the costs associated with the final volume capable tool will have already been absorbed at the prototype stage.

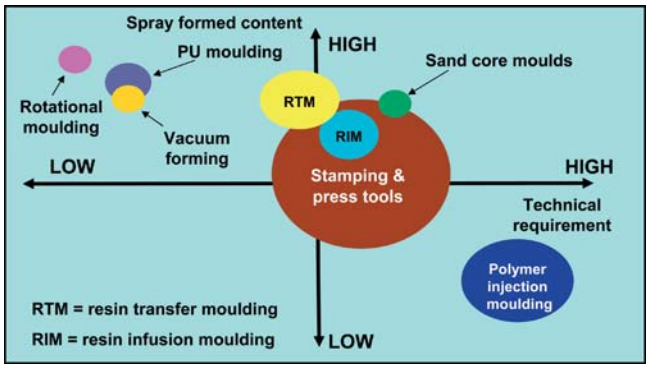

Fig. 11 The relative position of tooling markets in terms of the final spray form content and technical requirement

Fig. 12 A 800 by 600 mm spray formed steel shell for press tool applications, currently under assessment in volume production

7. Summary and Conclusions

To understand the complex spray forming process and to scale up the technology toward a full commercial format, a large interdisciplinary research team has been formed involving material scientists and control engineers at Oxford University in collaboration with the Ford Motor Company. A variety of experimental and modeling approaches have been used to understand the complex process physics, including IR thermal imaging, dynamic deflection measurements, real-time control of wire feed rate and shell temperature, particle image velocimetry of droplet splashing, shell heat flow and shape evolution modeling, and microstructural examination. A number of innovations have been made in the areas of off-line path planning, on-line thermal control, and microstructural understanding, particularly in the manipulation of phase transformations to control and eliminate residual stresses. The time and cost savings of spray formed steel tooling vary from segment to segment within the tooling market, and spray forming is not suitable for all market segments. Nonetheless, demonstrator tools for use in high-volume press tool applications have shown fit-for-purpose performance. It is envisaged that further innovations will enable the spray forming of tools to become a more important and widely adapted technology in toolmaking.

Acknowledgments

The authors would like to thank the UK Engineering and Physical Sciences Research Council and the Ford Motor Company for financial support.

References

1. B. Xu, X. Liu, S. Ma, and Z. Chen, The Experimental Study on Arc Sprayed Mouldmaking for Plastic Products, *Thermal Spray: Meeting the Challenges of the 21st Century* (Nice, France), May 25-29, 1998, C. Coddet, Ed., ASM International, 1998, p 1039-1042
2. M. Statham, E. Hammett, B. Harris, R.G. Cooke, R.M. Jordan, and A. Roche, Net-Shape Manufacture of Low-Cost Ceramic Shapes by Freeze-Gelation, *J. Sol-Gel Sci. Technol.,* 1998, **13,** p 171-173
3. A.P. Newbery, P.S. Grant, A.R. Roche, R.M. Jordan, and T. Carr, The Electric Arc Spray Manufacture of Rapid Production Tooling: A Case Study, *Thermal Spray: Meeting the Challenges of the 21st Century* (Nice, France), May 25-29, 1998, C. Coddet, Ed., ASM International, 1998, p 1223-1228
4. S. Hoile, T. Rayment, and P.S. Grant, Phase Transformations and Control of Residual Stresses in Thick Spray Formed Steel Shells, *Metall. Mater. Trans. B,* 2004, **35B,** p 1113-1122
5. P.D.A. Jones, S.R. Duncan, T. Rayment, and P.S. Grant, Optimal Robot Path for Minimizing Thermal Variations in a Spray Deposition Process, *IEEE Trans. Control Sys. Technol.,* accepted for publication
6. P.S. Grant, W.T. Kim, B.P. Bewlay, and B. Cantor, The Monitoring of Deposit Surface Temperatures During Spray Forming by Infrared Thermal Imaging, *Scr. Met.,* 1989, **23,** p 1651-1656
7. P.D.A. Jones, S.R. Duncan, T. Rayment, and P.S. Grant, Control of Temperature Profile for a Spray Deposition Process, *IEEE Trans. Control Sys. Technol.,* 2003, **11,** p 656-667
8. A.P. Newbery, P.S. Grant, and R.A. Neiser, The Velocity and Temperature of Steel Droplets During Electric Arc Spraying, *Surf. Coatings Technol.,* 2005, **195,** p 91-101
9. T. Rayment and P.S. Grant, Modelling the Heat Flow in Spray Formed Steel Shells for Tooling Applications, *Mater. Trans. B,* accepted for publication
10. A.P. Newbery and P.S. Grant, Droplet Splashing and Microstructure in Electric Arc Spraying, *J. Thermal Spray Technol.,* 2000, **9,** p 250-258
11. A.P. Newbery, T. Rayment, and P.S. Grant, A Particle Image Velocimetry Investigation of In-Flight and Deposition Behaviour of Steel Droplets During Electric Arc Spray Forming, *Mater. Sci. Eng. A,* 2004, **383,** p 137-145
12. Z. Djuric and P.S. Grant, Two Dimensional Simulation of Liquid Metal Spray Deposition onto a Complex Surface II: Splashing and Redeposition, *Model. Simul. Mater. Sci. Eng.,* 2001, **9,** p 111-127